Technische Universität Ilmenau
Institut für Mathematik

Preprint No. M **15/07**

Obstacle scanning by technical vibrissae with compliant support

Christoph Will, Joachim Steigenberger,
Carsten Behn

18. November 2015

Impressum:
Hrsg.: Leiter des Instituts für Mathematik
Weimarer Straße 25
98693 Ilmenau
Tel.: +49 3677 69-3621
Fax: +49 3677 69-3270
http://www.tu-ilmenau.de/math/

ilmedia

Obstacle scanning by technical vibrissae with compliant support

Christoph Will[*], **Joachim Steigenberger**[†], and **Carsten Behn**[*]

November 18, 2015

Abstract

Rodents, like mice and rats, use tactile hairs in the snout region (mystacial vibrissae) to acquire information about their environment, e.g. the shape or contour of obstacles. For this, the vibrissa is used for the perception of stimuli due to an object contact. Mechanoreceptors are processing units of this stimuli measured in the compliant support (follicle sinus complex). We use this behavior from biology as an inspiration to set up a mechanical model for object contour scanning. An elastic bending rod interacts with a rigid obstacle in the plane. Analyzing only one quasi-static sweep of the rod along the obstacle (in contrast to literature), we determine a) the support reactions (the only observables of the problem), and then b) the (discrete) obstacle contour in form of a set of contact points. In doing this, we first assume a stiff support (clamping) of the vibrissa, but in a next step we increase the elasticity of the support in focussing on a bearing with a rotational spring (also to control or delimitate the bending moment at the support). Thereby, we present a fully analytical treatment of the non-linear differential equations emerging from Bernoulli's rod theory and a representation by Standard Elliptic Integrals.

Keywords: vibrissa, sensing, object scanning, elastic support, contour reconstruction.
MSC[2010]: 34B60, 74K10, 74L15, 74M15, 92C10

1 Introduction

A challenging task in mobile robotics is to navigate in uncertain (e.g. changing, dark or noisy) environment. Optical sensors reach their capability in dark and/or noisy environments, such that tactile sensors get attracting attention. Because of technical solutions are often inspired by nature, we have a glance to the animal kingdom. Nocturnal animals like rodents (e.g. mice and rats) exhibit special tactile hairs in the snout region: the so-called mystacial vibrissae (Fig. 1), [Voges et al., 2012] and [Schmidt et al., 2014].

[*]Department of Technical Mechanics, Faculty of Mechanical Engineering, Ilmenau University of Technology, Max-Planck-Ring 12 (Building F), 98693 Ilmenau, Germany
[†]Institute of Mathematics, Ilmenau University of Technology, Weimarer Straße 25, 98693 Ilmenau, Germany

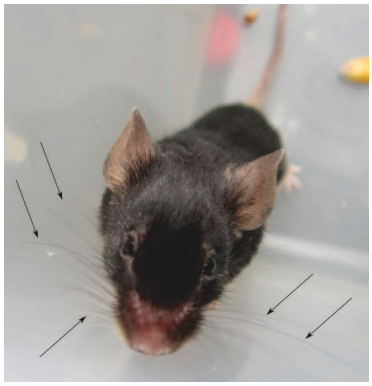

Figure 1: Mouse with vibrissae (see arrows), [Baldeweg et al., 2014].

These hairs are used to obtain information about the environment, whereby these vibrissae are used in very special modes: an active and passive one. These sensor hairs are supported in a compliant follicle sinus complex (FSC) as shown in Figure 2. Mechanoreceptors in and around the FSC can detect the movement of the vibrissa, e.g. of the vibrissa base, and convert this mechanical strain into signals to the central nervous system. The main difficulty is the fact, that the animals get only information about the environment from the processing mechanoreceptors. Hence, the challenge is to develop a mechanical model which serves for perception of information and processing of these as well.

Inspired by this biological paragon and motivated by its complex task to govern information, we focus on a vibrissa in passive mode, i.e., object localization. We set up a mechanical model in form of a plane elastic bending rod for a quasi-static obstacle scanning, whereby the rod is firstly supported by a clamp and then by a bearing including a rotational spring (to model the support compliance of the vibrissa in the FSC). The exploitation of the corresponding mathematical models is primarily not based on numerical methods, but it relies on an analytical framework as far as possible. Before doing this, we focus on the state of art to make a dissociation of the actual work in this field.

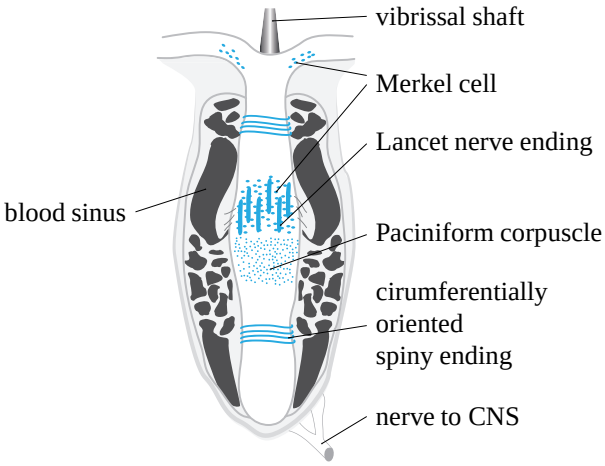

Figure 2: Follicle sinus complex [Behn, 2013], arranged by D. Voges (TU Ilmenau).

2 State of the Art

In recent years, bio-inspired technical vibrissae are used in mobile robotics, for example, for obstacle detection for path planning in [Kim and Möller, 2006], [Pearson et al., 2011], [Prescott et al., 2009]. For this, the literature exhibits various approaches in modeling such a technical vibrissa:

- Hirose et al. present in [Hirose et al., 1989] first models consisting of a long thin elastic beam for the detection of deformation of the vibrissa caused by an obstacle contact. The authors use the information of deformation, whereas the deformation of the vibrissa has to be large enough to exceed a given threshold, to mark a point on a map as an obstacle for further path-planning algorithms. Hence, they just focus on detection of obstacles.

- In [Kim and Möller, 2007] and [Tuna et al., 2012], further approaches are given which allow to obtain additional information about the obstacle. That is, in [Tuna et al., 2012], a contact point with an obstacle is estimated using the angle of deflection at the base (inspired by methods in computer tomography, ray deflection). Further on, in [Kim and Möller, 2007] the linear theory of elasticity is used in application to large deflections of a beam. In both methods, only the angle of deflection, neither forces nor moments, are measured.

- Another model is presented in [Birdwell et al., 2007]. There, both small deformations and the pre-curvature of the beam are taken into account. This is done in adding the pre-curvature to the linear deflection of the beam to get the actual position of the beam. This is a crude simplification of the problem. The achievable accuracy of the model depends on the pre-curvature of the beam, because the curvature is assumed to be a function on the beam axis. For small radii of sufficiently long beams, this method can fail due to the cartesian coordinate system. Also, it is still unclear, if the pre-curvature of the vibrissa results in a pre-stress.

- A further and improved method for object localization and shape detection is given in [Scholz and Rahn, 2004] for plane problems, and in [Clements and Rahn, 2006] for spatial problems. In both works, the authors switch from linear approximation of the curvature to the description of the problem in natural coordinates. This is a main improvement in comparison to previous works. Thus, they allow for large deflections of the beam, which results in a clear formulation of the boundary conditions (BCs). Further, experimental data are used in a numerical reconstruction algorithm in Simulink which results in the deformed beam shapes and a numerical values for the contact point. The entirety of all these beam shapes models the shape of the object geometry.

- Recent works, e.g. [Pammer et al., 2013], approximate the curvature of the beam in using finite differences. This gives the possibility to consider the curvatures of an undeformed vibrissa, but analytical equations with new insights do not exist due to only numerical simulations.

- Additional papers concerning a special perception of the environment as texture detection is close to the works focussing on scanning, but the authors focus on the active mode and analyze vibrations of the vibrissa-like rod, see [Boubenec et al., 2014] and [Quist et al., 2014].

- Contrary to the works mentioned above, we focussed on an analytical description of the profile scanning process using a technical vibrissa in [Will et al., 2014b]. The vibrissa was modeled as an elastic, one-sided clamped beam and we determined a sequence of contact points of the vibrissa with a profile in sweeping the vibrissa quasi-statically along this profile by *only one single sweep*, in contrast to [Scholz and Rahn, 2004]. The contact point is determined is using a developed reconstruction algorithm which is only based on the clamping reactions of the foot point of the technical vibrissa. This is due to the fact, that animals have to solely rely on the information from the mechanoreceptors at the follicle-sinus complex. Because of presently missing experiments, we focus on reconstruction problems of the profile contour in using noisy data (i.e., the clamping reactions are added with artificial measurement noise) in [Will et al., 2014a]. The investigations show up a good working reconstruction algorithm with reliable and good results.

3 Aim and Scope

Following the statements and evaluations from Sections 1 and 2, we focus on three topics which are new in literature:

1. A detailed consideration of the one-sweep scanning process when the vibrissa is clamped at its foot (preferred also in, e.g. [Neimark et al., 2003], [Scholz and Rahn, 2004], [Will et al., 2014a], [Will et al., 2014b]);
2. same investigation when the clamp is replaced by an elastic rotational pivot—thereby coming closer to the biological paragon FSC and enabling certain controls at the vibrissa foot;
3. since the boundary problems are autonomous we prefer a fully analytical treatment as far as possible, numerical results via evaluation of standard functions and solving nonlinear equations.

For this, we set up the general scanning problem in the next section, where we additionally state the main assumptions.

4 Modeling and Assumptions

We set up a mechanical model and investigate the quasi-static bending behavior, when the beam is swept along an obstacle from the right to the left, see Fig. 3.

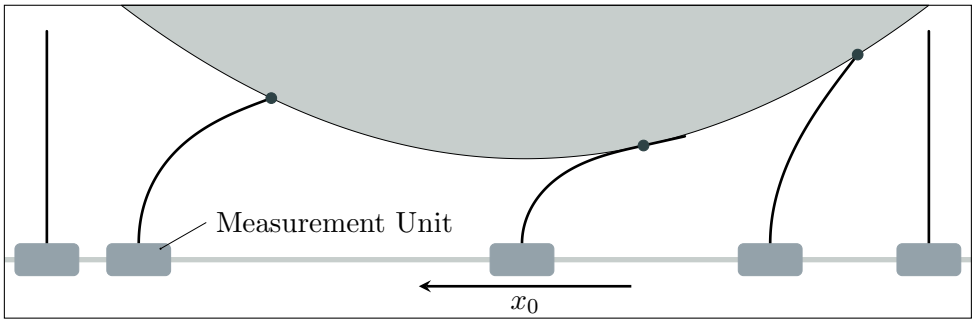

Figure 3: Scheme of profile scanning. • Contact point.

The following assumptions are taken essentially from [Will et al., 2014b]. They admit the announced analytical treatment (using Standard Elliptic Integrals) and allow to extend the results from [Will et al., 2014a] and [Will et al., 2014b].

- The problem is treated as a quasi-static one.
- We restrict the problem to an (x, y)-plane. The (originally undeformed) vibrissa is vertical, its base moves along the x-axis from the right to the left.
- The vibrissa is assumed as a long, slim, straight (until now, no pre-curvature is assumed) bending beam with constant second moment of area I_z, constant Young's modulus E and length L. The stress of the beam is sufficiently small to use Hooke's law of linear elasticity. Thus, ignoring shear stress, the Euler-Bernoulli theory for large deflections is applicable.
- The support of the beam is, at first (in Section 5), a clamp, later (in Section 6) a bearing with torsional spring due to the compliant properties of the FSC, see Figure 2.
- The obstacle contour (i.e., its boundary) is the graph of a strictly convex function $g : x \mapsto g(x)$, with $g \in \mathcal{C}^1(\mathbb{R}; \mathbb{R})$, having its minimum at $x = 0$.

- The object contact is ideal, i.e., the deformation of the beam is caused by a single contact force perpendicular to the obstacle profile. Friction is not taken into account, first attempts could be found in [Steigenberger et al., 2015].

Consider the constitutive law:

$$\kappa(s) = \frac{M_{bz}(s)}{EI_z}\,, \tag{4.1}$$

which is valid due to the assumptions.
Here, $M_{bz}(\cdot)$ denotes the bending moment with respect to the z-axis, $s \in [0, L]$ is the arc length of the beam, and $\kappa(\cdot)$ represents the curvatures, see Figure 4. For the sake of brevity, we introduce dimensionless variables. The units of measure are [length] $= L$, [moments] $= EI_zL^{-1}$ and [forces] $= EI_zL^{-2}$ (for example: $s = Ls^*\,,\ s^* \in [0, 1]$).

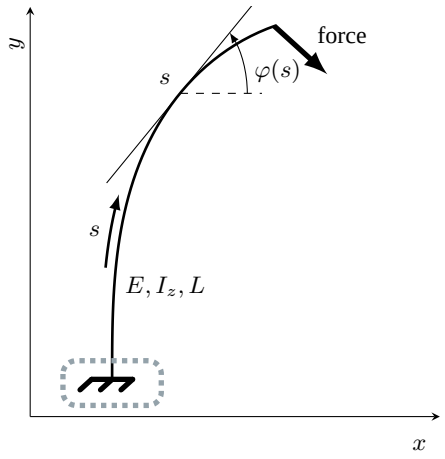

Figure 4: Euler-Bernoulli beam under large deflection, the "measurement unit" is dotted.

Now, all quantities are given in dimensionless representation, whereby the asterisk is dropped. Hence, (4.1) becomes

$$\kappa(s) = M_{bz}(s) \tag{4.2}$$

and the deformed beam (the elastic line) is parameterized by

$$\left.\begin{aligned} \frac{\mathrm{d}}{\mathrm{d}s}x(s) &= \cos\left(\varphi(s)\right)\,, \\ \frac{\mathrm{d}}{\mathrm{d}s}y(s) &= \sin\left(\varphi(s)\right)\,, \\ \frac{\mathrm{d}}{\mathrm{d}s}\varphi(s) &= \kappa(s)\,, \end{aligned}\right\}$$

with initial conditions $x(0) = x_0$, $y(0) = 0$ and $\varphi(0) = \frac{\pi}{2}$ (due to the clamping). Due to the strict convexity of g, x and y are functions of the slope angle α:

$$\begin{aligned} & \frac{\mathrm{d}}{\mathrm{d}x}g(x) = g'(x) = \tan(\alpha) \\ \Rightarrow \qquad & x = \xi(\alpha) \coloneqq g'^{-1}(\tan(\alpha))\,, \\ \Rightarrow \qquad & y = \eta(\alpha) \coloneqq g(\xi(\alpha))\,. \end{aligned}$$

Thus:

$$\big(x, g(x)\big) \mapsto \big(\xi(\alpha), \eta(\alpha)\big)\,, \quad \alpha \in \left(-\frac{\pi}{2}, \frac{\pi}{2}\right)\,.$$

Having a glance to Figure 5, it is obvious to distinguish two configurations of contacting the profile in order to formulate the BCs:

- Phase A: Contact of beam tip and profile with $\varphi(1) \geq \alpha$,
- Phase B: Contact of a point $s_1 \in (0,1)$ and the profile with equal angles $\varphi(s_1) = \alpha$.

In each phase, the contact point is given by the slope angle α of the profile.
Although both phases may occur in each vibrissa model (with stiff or elastic support), their analytical treatment are obviously different. Hence, we start analyzing both problems in separate sections in the following.

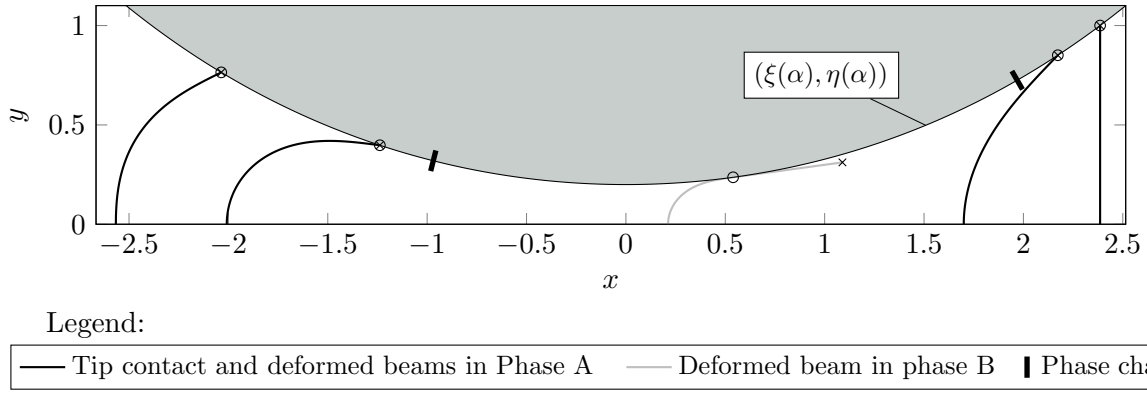

Figure 5: Profile with deflected beams.

5 Model I - Stiff support

5.1 Phase A: Contact at the Tip

Using Figure 6, the bending moment in this phase is, for $s \in (0,1)$:

$$M_{bz}(s) = f\Big(\big(y(s) - \eta(\alpha)\big)\sin(\alpha) + \big(x(s) - \xi(\alpha)\big)\cos(\alpha)\Big). \tag{5.3}$$

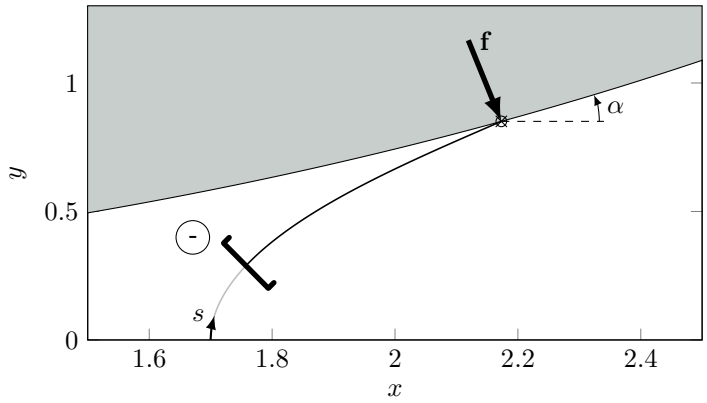

Figure 6: Deflected beam in Phase A.

To decouple the bending moment from $x(s)$ and $y(s)$, the derivative of (5.3) yields the following ODE system (5.4) with BCs (5.5):

$$\begin{array}{|ll|ll|} \hline \text{(a)} & \kappa'(s) = f\cos(\varphi(s) - \alpha) & \text{(c)} & x'(s) = \cos(\varphi(s)) \\ \text{(b)} & \varphi'(s) = \kappa(s) & \text{(d)} & y'(s) = \sin(\varphi(s)) \\ \hline \end{array} \tag{5.4}$$

(a)	$\varphi(0) = \frac{\pi}{2}$	(c)	$\kappa(1) = 0$	(e)	$y(1) = \eta(\alpha)$
(b)	$y(0) = 0$	(d)	$x(1) = \xi(\alpha)$		

(5.5)

This BVP splits into two separate problems: {(5.4a,b),(5.5a,c)} and {(5.4c,d),(5.5b,d,e)}. The first one has

$$\kappa^2 = 2f\left(\sin(\varphi - \alpha) - \sin(\varphi_1 - \alpha)\right) \tag{5.6a}$$

$$= 4f \sin\left(\frac{\varphi - \varphi_1}{2}\right) \cos\left(\frac{\varphi + \varphi_1 - 2\alpha}{2}\right) . \tag{5.6b}$$

as a first integral with $\varphi_1 \coloneqq \varphi(1)$.
Note that the bending moment, considering the lower part of the beam, depends on the clamping reactions M_z, F_x, F_y, which results in a first integral of the form:

$$\kappa^2 = 2f \sin(\varphi - \alpha) - 2f \cos(\alpha) + M_z^2 .$$

Because $\kappa^2(s) \geq 0$ has to be fulfilled for every $s \in [0, 1]$, three cases have to be discussed for (5.6b) with $f > 0$:

1. At least one factor is zero: hence $\kappa(s) \equiv 0$, and the beam is not deformed at all.

2. Both factors are negative: The sine function is positive on the interval $(-\pi, 0)$ and negative on $(\pi, 2\pi)$. This results in the inequations

   $$-2\pi < \varphi(s) - \varphi_1 < 0 \quad \vee \quad 2\pi < \varphi(s) - \varphi_1 < 4\pi .$$

   Hence $\varphi(s) < \varphi_1 \vee \varphi(s) > 2\pi$. This is a **contradiction**, because $\varphi(s) \in \left[\varphi_1, \frac{\pi}{2}\right] \ \forall s \in [0, 1]$.

3. Both factors are positive: The sine function is positive on the domain $(0, \pi)$, the cosine function on $\left(-\frac{\pi}{2}, \frac{\pi}{2}\right)$. Therefore, it must hold:

   $$0 < \varphi(s) - \varphi_1 < 2\pi \ \wedge \ -\pi < \varphi(s) + \varphi_1 - 2\alpha < \pi .$$

   The first inequality contains no additional information, the second one yields:

   $$\begin{aligned} & \varphi(s) + \varphi_1 < \pi + 2\alpha \ \forall s \\ \Rightarrow \qquad & \varphi_1 < \frac{\pi}{2} + 2\alpha, \quad \text{since} \quad \varphi(s) \leq \frac{\pi}{2} . \end{aligned}$$

Therefore, the angle φ_1 has to be in the domain $\alpha < \varphi_1 < \min\left(\left\{\frac{\pi}{2}, \frac{\pi}{2} + 2\alpha\right\}\right)$.
Due to the assumptions, the curvature is non-positive along the solutions of (5.4a,b), which results in, using (5.6a):

$$\frac{\mathrm{d}\varphi(s)}{\mathrm{d}s} = \kappa(s) = -\sqrt{2f}\sqrt{\sin(\varphi(s) - \alpha) - \sin(\varphi_1 - \alpha)} =: \varkappa(\varphi; f, \varphi_1, \alpha) \tag{5.7}$$

as an ODE with separated variables for $\varphi(s)$. Integration of (5.7) together with condition (5.5a) yields

$$\sqrt{2f}s = K(\varphi, \varphi_0, \varphi_1, \alpha) \coloneqq -\int_{\varphi_0}^{\varphi} \left(\sin(t - \alpha) - \sin(\varphi_1 - \alpha)\right)^{-\frac{1}{2}} \mathrm{d}t \tag{5.8}$$

This integral can be rewritten with the help of Standard Elliptic Integrals, which is shown in Appendix A. At the moment, it suffices to see it as a well defined function K of $(\varphi, \varphi_0, \varphi_1, \alpha)$ with $\varphi_0 = \frac{\pi}{2}$. By using $s = 1$ and therefore $\varphi(1) = \varphi_1$, a crucial conclusion is:

$$f = \frac{1}{2} K^2\left(\varphi_1, \frac{\pi}{2}, \varphi_1, \alpha\right) . \tag{5.9}$$

The further solution of the ODE system (5.4), namely (5.4c,d), can be achieved in a neat way by applying a variable transformation: replacing the arc length s with the slope angle φ. To guarantee the uniqueness of the transformation, $\varphi(s)$ must be monotonic. This property is provided by (5.7): $\varphi(s)$ is monotonically decreasing from $\frac{\pi}{2}$ to φ_1.
We now get the transformed ODE system and initial conditions

$$\boxed{\begin{array}{llll} \text{(a)} & \dfrac{\mathrm{d}x}{\mathrm{d}\varphi} = \dfrac{\cos(\varphi)}{\varkappa\left(\varphi; f, \varphi_1, \alpha\right)}\,, & \text{(c)} & x\left(\dfrac{\pi}{2}\right) = x_0\,, \\ \text{(b)} & \dfrac{\mathrm{d}y}{\mathrm{d}\varphi} = \dfrac{\sin(\varphi)}{\varkappa\left(\varphi; f, \varphi_1, \alpha\right)}\,, & \text{(d)} & y\left(\dfrac{\pi}{2}\right) = 0\,. \end{array}} \tag{5.10}$$

Finally, we have

$$x = X\left(\varphi; f, \frac{\pi}{2}, \varphi_1, \alpha\right) \coloneqq -\frac{1}{\sqrt{2f}} \int\limits_{\frac{\pi}{2}}^{\varphi} \frac{\cos(t)}{\sqrt{\sin(t-\alpha) - \sin(\varphi_1 - \alpha)}}\,\mathrm{d}t\,, \tag{5.11}$$

$$y = Y\left(\varphi; f, \frac{\pi}{2}, \varphi_1, \alpha\right) \coloneqq -\frac{1}{\sqrt{2f}} \int\limits_{\frac{\pi}{2}}^{\varphi} \frac{\sin(t)}{\sqrt{\sin(t-\alpha) - \sin(\varphi_1 - \alpha)}}\,\mathrm{d}t\,. \tag{5.12}$$

The only unknown parameter left is φ_1. Using BC (5.5e) we get

$$Y\left(\varphi_1; \frac{1}{2}K^2\left(\varphi_1, \frac{\pi}{2}, \varphi_1, \alpha\right), \frac{\pi}{2}, \varphi_1, \alpha\right) - \eta(\alpha) = 0\,, \tag{5.13}$$

which can be solved numerically for φ_1 with $\varphi_1 \in \left(\alpha, \min\left\{\frac{\pi}{2}, \frac{\pi}{2} + 2\alpha\right\}\right)$. The deformed beam is then described in the xy-plane with respect to the slope angle by

$$\begin{aligned} x &= \xi(\alpha) - X\left(\varphi_1; f, \frac{\pi}{2}, \varphi_1, \alpha\right) + X\left(\varphi; f, \frac{\pi}{2}, \varphi_1, \alpha\right)\,,\ \varphi \in \left[\varphi_1, \frac{\pi}{2}\right], \\ y &= Y\left(\varphi; f, \frac{\pi}{2}, \varphi_1, \alpha\right)\,. \end{aligned}$$

5.2 Phase B: Tangential Contact

The bending moment is now, with yet unknown contact point s_1 (see Figure 7):

$$M_{bz}(s) = \begin{cases} f\Big(\big(y(s) - \eta(\alpha)\big)\sin(\alpha) + \big(x(s) - \xi(\alpha)\big)\cos(\alpha)\Big), & s \in (0, s_1] \\ 0, & s \in (s_1, 1)\,. \end{cases} \tag{5.14}$$

While the ODE-system (5.4) stays the same, the related BVP with $s \in (0, s_1)$ now is:

$$\boxed{\begin{array}{lll} \text{(a)} \quad \varphi(0) = \frac{\pi}{2} & \text{(c)} \quad \kappa(s_1) = 0 & \text{(e)} \quad x(s_1) = \xi(\alpha) \\ \text{(b)} \quad y(0) = 0 & \text{(d)} \quad \varphi(s_1) = \alpha & \text{(f)} \quad y(s_1) = \eta(\alpha) \end{array}} \tag{5.15}$$

With respect to the new BC, the first integral of (5.4a), (5.4b), and (5.15c) is:

$$\begin{aligned} \kappa^2 &= 2f\sin(\varphi - \alpha) \\ \Rightarrow \quad \frac{\mathrm{d}}{\mathrm{d}s}\varphi(s) = \kappa(s) &= -\sqrt{2f}\sqrt{\sin(\varphi(s) - \alpha)} = \varkappa(\varphi; f, \alpha, \alpha)\,. \end{aligned} \tag{5.16}$$

Analogue to (5.8), we can now write, using (5.15d),

$$\sqrt{2f}s = K\left(\varphi, \frac{\pi}{2}, \alpha, \alpha\right)\,. \tag{5.17}$$

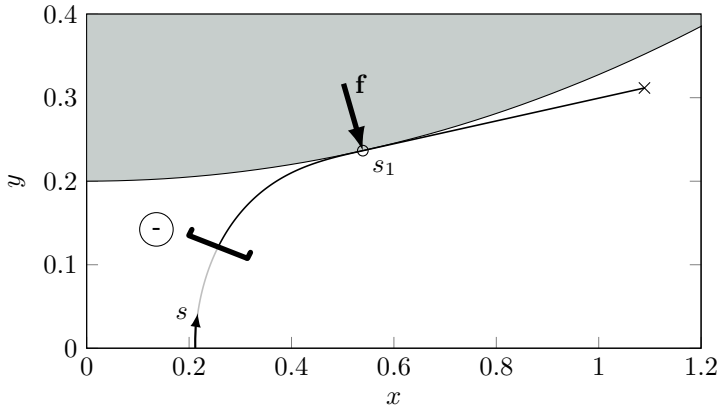

Figure 7: Deflected beam in Phase B, contact $s_1 \in (0, 1)$.

Unlike Phase A, we can only conclude

$$f = \frac{1}{2\,{s_1}^2} K^2 \left(\alpha, \frac{\pi}{2}, \alpha, \alpha\right) , \tag{5.18}$$

which still has the unknown arc length s_1 in it. As with φ_1 in Phase A, the BC which resolves this is the contact point in y-direction (5.15f):

$$Y\left(\alpha, \frac{1}{2\,{s_1}^2} K^2 \left(\alpha, \frac{\pi}{2}, \alpha, \alpha\right), \frac{\pi}{2}, \alpha, \alpha\right) - \eta(\alpha) = 0\,. \tag{5.19}$$

Equation (5.19) can be explicitly solved for s_1 (with placeholder variable t to not write the lengthy term in the denominator, see Appendix A:

$$s_1 = \frac{\eta(\alpha) K\left(\alpha, \frac{\pi}{2}, \alpha, \alpha\right)}{\sqrt{2t}\, Y\left(\alpha, t, \frac{\pi}{2}, \alpha, \alpha\right)}\,. \tag{5.20}$$

Again, all unknown parameters are now known and the x- and y-coordinate of the beam is

$$\begin{aligned} x &= \xi(\alpha) - X\left(\alpha; f, \frac{\pi}{2}, \alpha, \alpha\right) + X\left(\varphi; f, \frac{\pi}{2}, \alpha, \alpha\right) , \\ y &= Y\left(\varphi; f, \frac{\pi}{2}, \alpha, \alpha\right) \qquad \varphi \in \left[\alpha, \frac{\pi}{2}\right] . \end{aligned}$$

The results of a sweep along an obstacle is detailed shown in [Will et al., 2014a] and [Will et al., 2014b]. Here only a short view is giving: Figure 8 shows the obstacle and the deformed beams, Figs. 9 and 10 clamping moment and clamping forces, respectively.

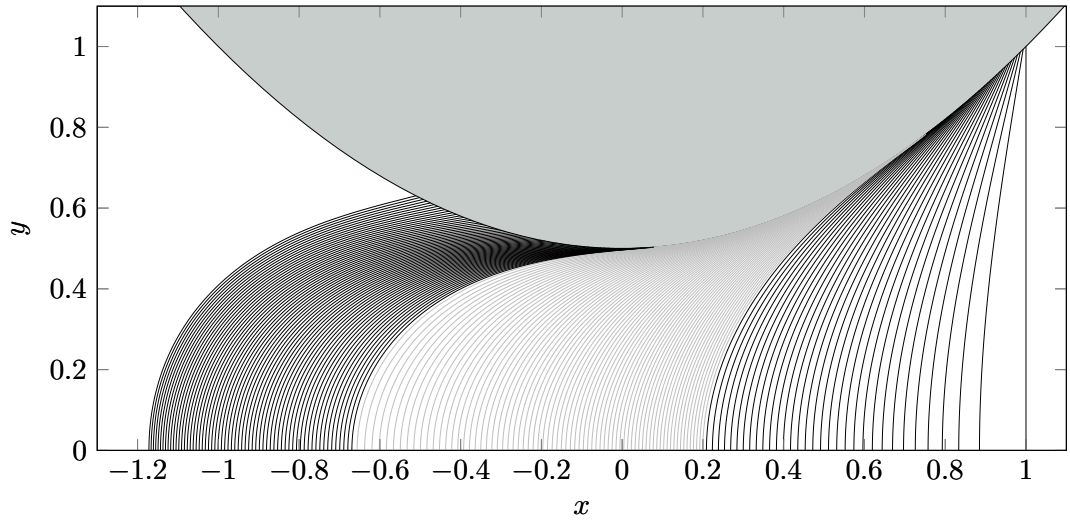

Figure 8: Deformed beams using profile contour function $g : x \mapsto \frac{1}{2}x^2 + \frac{1}{2}$.

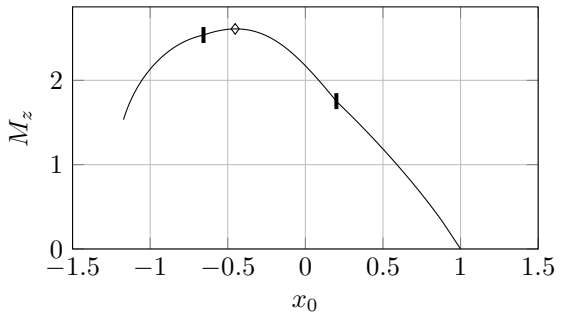

Figure 9: Clamping moment M_z (maximum marked with $\diamond$).

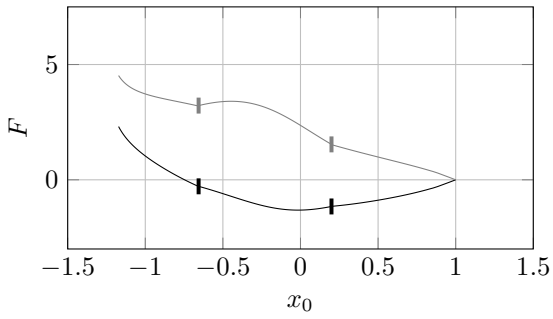

Figure 10: Clamping forces F: — F_x, — F_y, ❙ marks the change between Phase A and Phase B.

5.3 Reconstruction

We now have all tools at hand to generate the observables an animal relays on during exploration of unknown objects with its vibrissae. The next step is to use these data sets to reconstruct a contact point and, doing this repeatedly, gain a sequence of contact points representing the discrete profile contour. In previous work, we have used quadrature resp. formulated an initial value problem to get the contact point. In the present work, we present an analytical solution once the observables are available.

The describing ODE system does not change, so (5.4) is still a valid description of the problem. But, instead of solving a BVP (due to the fact that there is no boundary at which all necessary values are given), we have now all data available at the base point $s = 0$:

$$\boxed{\kappa(0) = \lim_{s\to 0+} M_{bz}(s) = -M_z\,, \qquad \varphi(0) = \frac{\pi}{2}\,, \qquad x(0) = x_0\,, \qquad y(0) = 0\,,}$$

and

$$\alpha = -\arctan\left(\frac{F_x}{F_y}\right)\,, \qquad f = \sqrt{F_x^2 + F_y^2}\,.$$

The main difficulty is to decide which phase the beam actually undergoes. To solve this, let us focus on the curvature (in Phase A, Phase B, or somewhere):

$$\text{Phase A: } \kappa_A^2(s) = 2f\left(\sin(\varphi(s) - \alpha) - \sin(\varphi_1 - \alpha)\right)\,, \tag{5.21}$$

$$\text{any } s\text{: } \quad \kappa_R^2(s) = 2f\left(\sin(\varphi(s) - \alpha) - \cos(\alpha)\right) + M_{Az}^2\,, \tag{5.22}$$

$$\text{Phase B: } \kappa_B^2(s) = 2f\sin(\varphi(s) - \alpha)\,. \tag{5.23}$$

Obviously, it is Phase B iff $\varphi_1 = \alpha$. Using (5.22), φ_1 can be determined by:

$$\varphi_1 = \alpha - \arcsin\left(\frac{M_z^2 - 2f\cos(\alpha)}{2f}\right)\,, \tag{5.24}$$

which results in the decision condition for Phase B with only known parameters:

$$\boxed{M_z^2 - 2F_y = 0\,.} \tag{5.25}$$

If (5.25) is valid, the contact force is applied at $s_1 \in (0, 1)$ which can be computed using (5.18):

$$s_1 = \frac{1}{\sqrt{2f}}\,K\left(\alpha, \frac{\pi}{2}, \alpha, \alpha\right)\,.$$

Else, if (5.25) does not hold, the contact force is applied at $s_1 = 1$ with φ_1 from (5.24). The contact point $(x(s_1), y(s_1))$ and, if necessary, any point of the deformed beam can now be calculated using the formulas $X(\cdot)$ and $Y(\cdot)$ from Appendix A.

To measure the quality of the reconstruction we define a error function as follows (Euclidian vector norm)

$$\text{error} := \left\| \begin{pmatrix} x_k(\varphi_{1k}) \\ y_k(\varphi_{1k}) \end{pmatrix} - \begin{pmatrix} \xi(\alpha_k) \\ \eta(\alpha_k) \end{pmatrix} \right\|_2,$$

where k is the k-th point at which the quasi-static deformation is calculated.

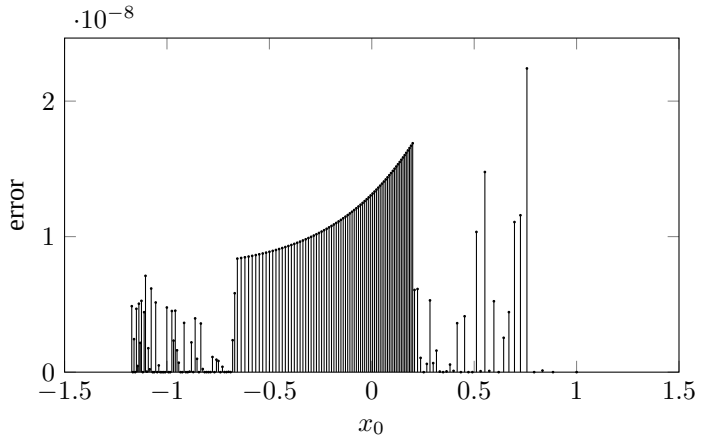

Figure 11: Reconstruction error for profile $g : x \mapsto \frac{1}{2}x^2 + \frac{1}{2}$.

6 Model II - Elastic Support

In Subsection 5.3, we showed that it is possible to reconstruct the contact point of beam and obstacle with only the information available at the base of the beam. But, with respect to more realistic supports, where moments have to be measured for the reconstruction, new models shall exhibit elastic supports as, e.g. a bearing with a torsional spring, which have to be taken into account. The new model is presented in Figure 12.

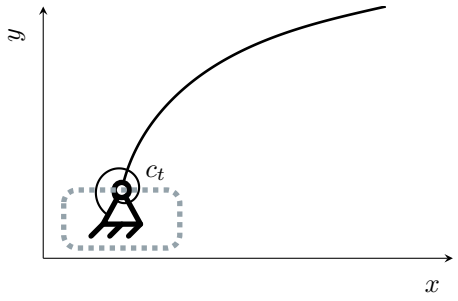

Figure 12: Model II: Euler-Bernoulli beam with elastic support.

As with Model I in Section 5 and given in Figure 4, the sweep of the beam along the obstacle can split into the two phases already mentioned there.

6.1 Phase A: Contact at the Tip

The principle way of handling the problem is the same, (5.3) and (5.4) as well. The BCs are now:

$$\boxed{\begin{array}{lll} \text{(a)} \quad \kappa(0) = c_t\left(\varphi_0 - \frac{\pi}{2}\right) & \text{(c)} \quad \kappa(1) = 0 & \text{(e)} \quad y(1) = \eta(\alpha) \\ \text{(b)} \quad y(0) = 0 & \text{(d)} \quad x(1) = \xi(\alpha) & \end{array}} \tag{6.26}$$

Starting with the curvature, which again is

$$\kappa(s) = -\sqrt{2f}\sqrt{\sin(\varphi(s) - \alpha) - \sin(\varphi_1 - \alpha)}\,, \tag{6.27}$$

the deflection angle at the base φ_0 can be calculated using (6.26a) and (6.27):

$$0 = \frac{\pi}{2} - \varphi_0 - \frac{\sqrt{2f}\sqrt{\sin(\varphi_0 - \alpha) - \sin(\varphi_1 - \alpha)}}{c_t}\,. \tag{6.28}$$

This leads to an expression for the contact force:

$$f = \frac{1}{2}K^2\left(\varphi_1, \varphi_0, \varphi_1, \alpha\right)\,. \tag{6.29}$$

With the already known transformation for $x'(s)$ and $y'(s)$ and using (6.26e), we now have the following nonlinear system to solve for φ_0 and φ_1, in order to have all parameters at hand:

$$\begin{aligned} 0 &= Y\left(\varphi_1; \frac{1}{2}K^2\left(\varphi_1, \varphi_0, \varphi_1, \alpha\right), \varphi_0, \varphi_1, \alpha\right) - \eta(\alpha)\,, \\ 0 &= \frac{\pi}{2} - \varphi_0 - \frac{\sqrt{2f}\sqrt{\sin(\varphi_0 - \alpha) - \sin(\varphi_1 - \alpha)}}{c_t}\,. \end{aligned} \tag{6.30}$$

The solution then is

$$\begin{aligned} x &= \xi(\alpha) - X\left(\varphi_1; f, \varphi_0, \varphi_1, \alpha\right) + X\left(\varphi; f, \varphi_0, \varphi_1, \alpha\right)\,,\ \varphi \in [\varphi_1, \varphi_0]\,, \\ y &= Y\left(\varphi; f, \varphi_0, \varphi_1, \alpha\right)\,. \end{aligned}$$

6.2 Phase B: Tangential Contact

Like with Phase A, only minor changes in the equations occur. The bending moment does not change, the new BC are:

$$\boxed{\begin{array}{lll} \text{(a)} \quad \kappa(0) = c_t\left(\varphi_0 - \frac{\pi}{2}\right) & \text{(c)} \quad \kappa(s_1) = 0 & \text{(e)} \quad x(s_1) = \xi(\alpha) \\ \text{(b)} \quad y(0) = 0 & \text{(d)} \quad \varphi(s_1) = \alpha & \text{(f)} \quad y(s_1) = \eta(\alpha) \end{array}} \tag{6.31}$$

With an expression for the curvature

$$\kappa = -\sqrt{2f}\sqrt{\sin(\varphi - \alpha)}\,, \tag{6.32}$$

we get again an equation to identify φ_0 under consideration of (6.31a):

$$0 = \frac{\pi}{2} - \varphi_0 - \frac{\sqrt{2f}\sqrt{\sin(\varphi_0 - \alpha)}}{c_t} \tag{6.33}$$

Again, it must hold

$$\sqrt{2f}\,s = K\left(\varphi, \varphi_0, \alpha, \alpha\right)\,.$$

So, the contact force is – again – an expression of the contact point s_1:

$$f = \frac{1}{2\,{s_1}^2} K^2\left(\alpha, \varphi_0, \alpha, \alpha\right) \,, \tag{6.34}$$

With (6.31f) we get

$$Y\left(\alpha, \frac{1}{2\,{s_1}^2} K^2\left(\alpha, \varphi_0, \alpha, \alpha\right), \varphi_0, \alpha, \alpha\right) - \eta(\alpha) = 0\,. \tag{6.35}$$

Since (6.28) can not be solved for φ_0 and has f in it, both, (6.35) and (6.28), needs to be solved together.

The final solution then is

$$\begin{aligned} x &= \xi(\alpha) - X\left(\varphi_1; f, \varphi_0, \varphi_1, \alpha\right) + X\left(\varphi; f, \varphi_0, \varphi_1, \alpha\right) \,,\ \varphi \in [\varphi_1, \varphi_0]\,, \\ y &= Y\left(\varphi; f, \varphi_0, \varphi_1, \alpha\right) \,. \end{aligned}$$

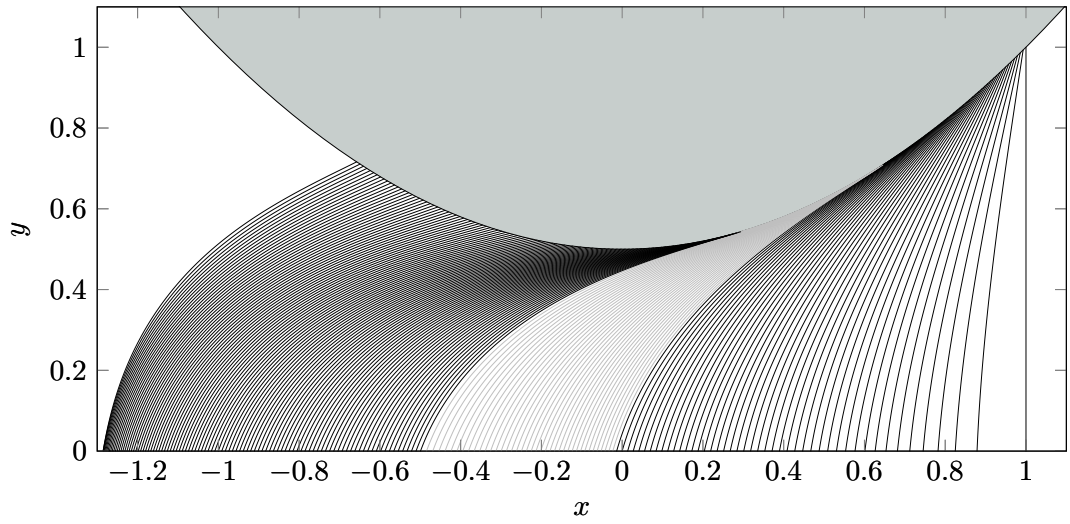

Figure 13: Deformed beams using profile contour function $g : x \mapsto \frac{1}{2}x^2 + \frac{1}{2}$ with $c_t = 5$.

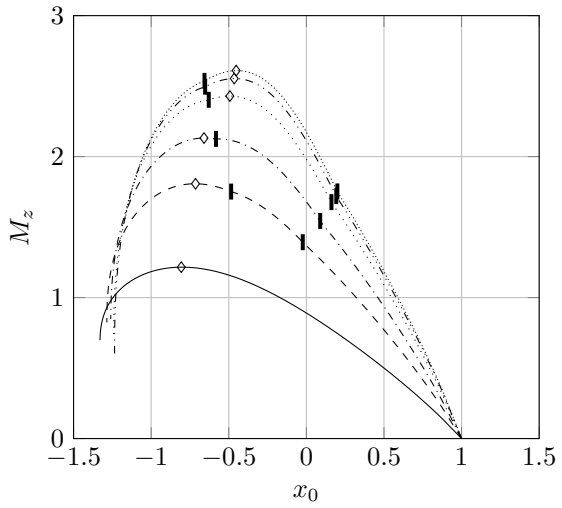

Figure 14: Torque of the torsional spring M_z (maximum marked with ⋄).

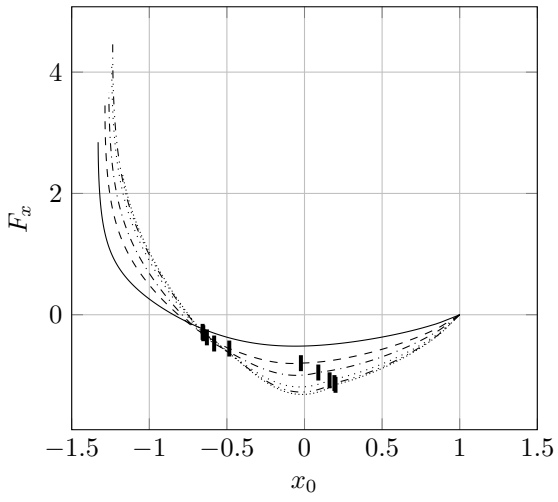

Figure 15: Support forces F_x, ❙ marks the change between Phase A and Phase B.

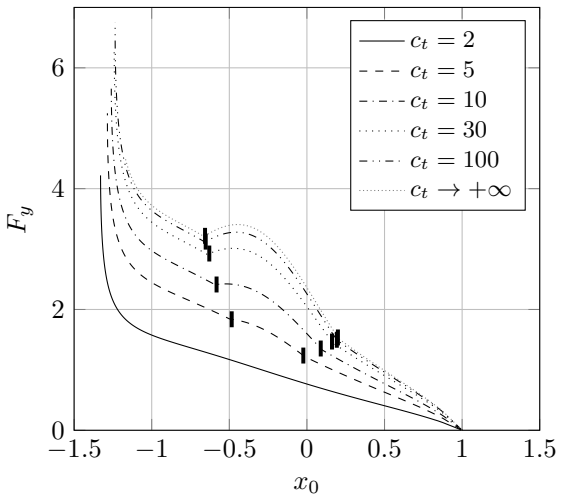

Figure 16: Support forces F_y, ❙ marks the change between Phase A and Phase B.

In Figure 14, the bending moment at the base point is shown. The graph shows the expected result: the maximum bending moment is reduced, if the support is relaxed. For $c_t = 2$ another effect occurs: while all other simulations show a Phase B, here only Phase A arises. This behavior is strongly depending on the profile contour, and therefore, is not always possible. The reaction force in y and x is shown in Figures 15 and 16, respectively. There, the same behavior occurs: the maximum value is reduced if the support is relaxed. But especially, the maximum of F_x is not reduced by the same amount as the bending moment gathered by the torsional spring. The deformed beams for $c_t = 5$ are shown in Figure 13.

6.3 Reconstruction

The reconstruction is quite similar to Model I described in Subsection 5.3. The observables needed to reconstruct a contact point are now

$$\boxed{c_t\,, \qquad \varphi(0) = \varphi_0\,, \qquad x(0) = x_0\,, \qquad y(0) = 0\,.}$$

The only additional information is

$$M_z = c_t \left(\frac{\pi}{2} - \varphi_0\right)$$

and

$$\varphi_1 = \alpha - \arcsin\left(\frac{M_z^2 - 2f\sin(\varphi_0 - \alpha)}{2f}\right). \tag{6.36}$$

The reconstruction error is shown in Figure 17. As with Model I, the reconstruction error is below $2 \cdot 10^{-8}$ and, therefore, of the same order of magnitude.

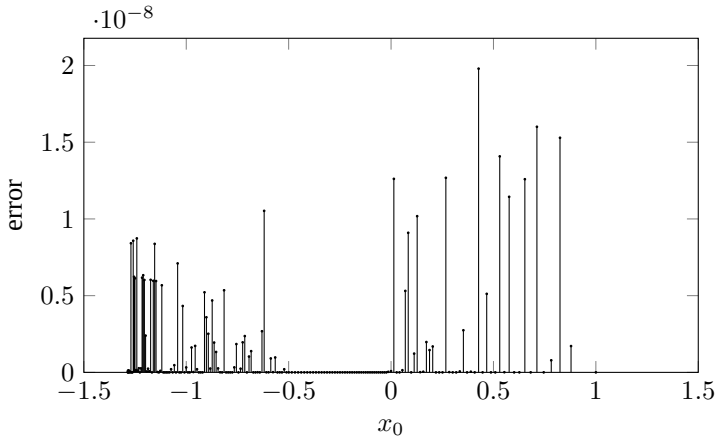

Figure 17: Reconstruction error for profile $g : x \mapsto \frac{1}{2}x^2 + \frac{1}{2}$.

6.4 Application: Stiffness Control

To gain an advantage of the model in Section 6, we now consider a controllable stiffness of the rotational spring during the sweep. For the biological paradigm imagine the following: a rat wants to pass a small tube-alike hole. After a short investigation using its mystacial vibrissa, it decides the hole's diameter is large enough to pass trough. While passing the hole, all vibrissae are bent and can not give new information, because the rat already decided it can pass through. Why should it invest energy and tense up its muscle to force the vibrissae to stay in a special angle? Instead it is sufficient to generate a specified torque by the musculature to enforce a contact between hair and hole in order to decide when the hole ends.

This is going to be realized in the following way: Instead of a torsional spring with constant stiffness, we replace it by one with controllable stiffness. Again, we get $M_z = c_t\left(\frac{\pi}{2} - \varphi_0\right)$, but only until a threshold $\overline{M_z}$ is reached. If so, the spring generates the constant moment $\overline{M_z}$ until $M_z \leq \overline{M_z}$: $M_z = \max\left(c_t\left(\frac{\pi}{2} - \varphi_0\right), \overline{M_z}\right)$.

The sweep can split into two phases again. In the following, we restrict ourself to the case $M_z = \overline{M_z}$ (see Section 6 for $M_z < \overline{M_z}$).

6.4.1 Phase A: Contact at tip

The BCs are

$$\boxed{\begin{array}{lll} \text{(a)} \quad \kappa(0) = -\overline{M_z} & \text{(c)} \quad \kappa(1) = 0 & \text{(e)} \quad y(1) = \eta(\alpha) \\ \text{(b)} \quad y(0) = 0 & \text{(d)} \quad x(1) = \xi(\alpha) & \end{array}} \tag{6.37}$$

The curvature is

$$\kappa(s) = -\sqrt{2f}\sqrt{\sin\left(\varphi(s) - \alpha\right) - \sin\left(\varphi_1 - \alpha\right)}\,.$$

So (6.37a) yields

$$\varphi_0 = \alpha + \arcsin\left(\frac{\overline{M_z}^2}{2f} + \sin\left(\varphi_1 - \alpha\right)\right)\,. \tag{6.38}$$

Hence, the contact force here is

$$f = \frac{1}{2}K^2(\varphi_1, \varphi_0, \varphi_1, \alpha)\,. \tag{6.39}$$

The BC (6.37e) with (6.38) and (6.39) results in the following system:

$$0 = \varphi_0 - \alpha - \arcsin\left(\frac{\overline{M_z}^2}{K^2(\varphi_1, \varphi_0, \varphi_1, \alpha)} + \sin(\varphi_1 - \alpha)\right),$$
$$0 = Y\left(\varphi_1; \frac{1}{2}K^2\left(\varphi_1, \varphi_0, \varphi_1, \alpha\right), \varphi_0, \varphi_1, \alpha\right) - \eta(\alpha)$$

with unknowns φ_0 and φ_1.

6.4.2 Phase B: Tangential Contact

The BC are

(a)	$\kappa(0) = -\overline{M_z}$	(c)	$\kappa(s_1) = 0$	(e)	$x(s_1) = \xi(\alpha)$
(b)	$y(0) = 0$	(d)	$\varphi(s_1) = \alpha$	(f)	$y(s_1) = \eta(\alpha)$

(6.40)

The curvature is

$$\kappa(s) = -\sqrt{2f}\sqrt{\sin(\varphi(s) - \alpha)}.$$

The BC (6.40a) yields

$$\varphi_0 = \alpha + \arcsin\left(\frac{\overline{M_z}^2}{2f}\right).$$

The force then is

$$f = \frac{1}{2{s_1}^2}K^2(\alpha, \varphi_0, \alpha, \alpha). \tag{6.41}$$

Therefore, we need to solve the following with unknowns φ_0 and s_1:

$$0 = \varphi_0 - \alpha - \arcsin\left(\frac{\overline{M_z}^2}{2f}\right),$$
$$0 = Y(\alpha; f, \varphi_0, \alpha, \alpha) - \eta(\alpha)$$

In the following, two variants are presented. In Figures 18 and 19, the bending moment and support forces for only a slight cap of the bending moment are shown. In this case, the torsional spring constant is $c_t = 100$ and the maximum bending moment is $\overline{M_z} = 2.4$.

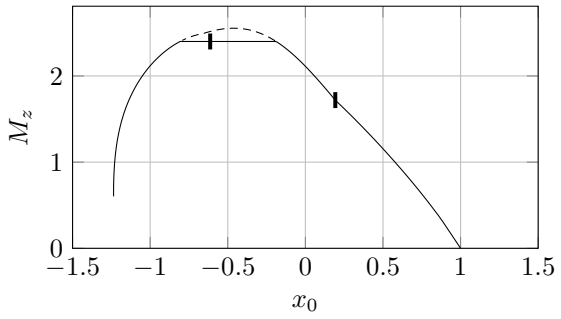

Figure 18: Torque of the torsional spring M_z with $c_t = 100$ and $\overline{M_z} = 2.4$ (dashed without stiffness control).

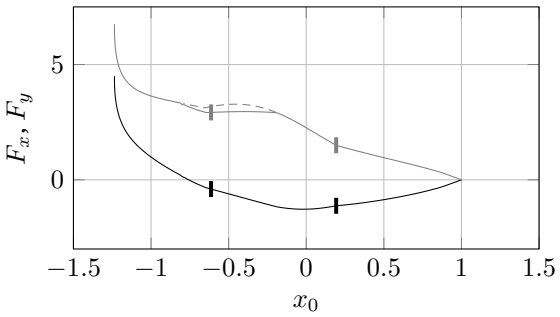

Figure 19: Clamping forces with $c_t = 100$ and $\overline{M_z} = 2.4$: — F_x, — F_y, ❙ marks the change between Phase A and Phase B.

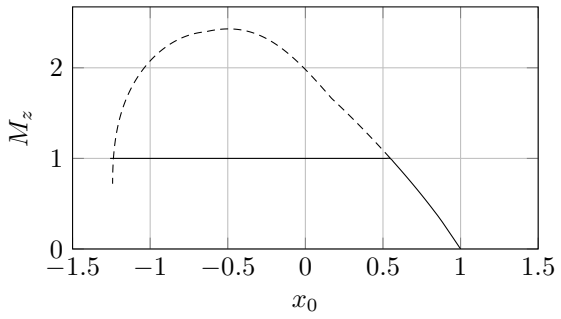

Figure 20: Torque of the torsional spring M_z with $c_t = 30$ and $\overline{M_z} = 1$ (dashed without stiffness control).

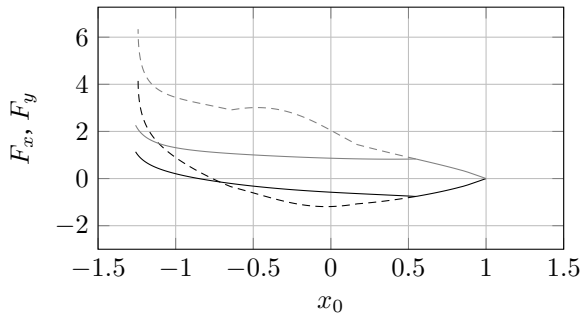

Figure 21: Clamping forces with $c_t = 30$ and $\overline{M_z} = 1$: — F_x, — F_y, ❙ marks the change between Phase A and Phase B.

The other case, shown in Figures 20 and 21, shows a situation where the bending moment is strongly capped, by restricting it to $\overline{M_z} = 1$. In this sweep, only Phase A occurs (see Figures 14 to 16 for comparison) and the bending moment stays at $M_z = 1$ until the snap off of the beam.

6.4.3 Reconstruction

The reconstruction does not differ from Subsection 6.3, except it needs to be known, when $\overline{M_z}$ is active. The result for $c_t = 30$ and $\overline{M_z} = 1$ is shown in Figure 22.

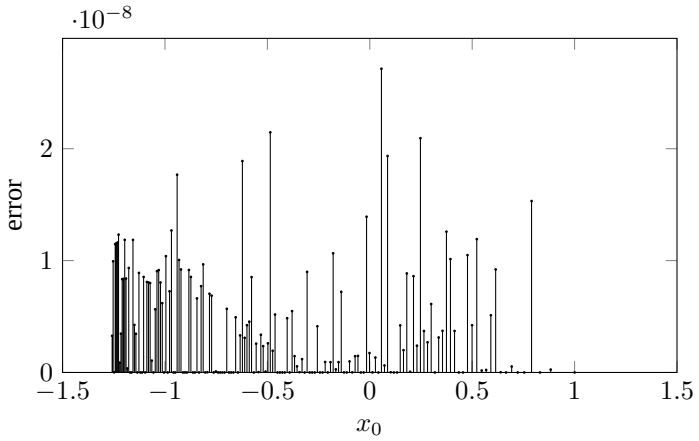

Figure 22: Reconstruction error for profile $g : x \mapsto \frac{1}{2}x^2 + \frac{1}{2}$.

7 Conclusion

To model the intelligent sensor system “animal vibrissa” which allows the animal to perceive the environment in form of, e.g. object contour scanning, we have set up two mechanical models. The first, introductory model presents a one-sided clamped Euler-Bernoulli bending rod, the other a more realistic model with a bearing and torsional spring instead of the clamping. Both models were used in theoretical application for scanning the obstacle boundary by only one sweep along it. The first challenging part was to determine the observables of the scanning process, i.e., the support reactions and the foot point of the vibrissa. This was done in solving the emerging boundary-value problem which solution was treated in a purely analytical way like using Standard Elliptic Integrals. In a second step, the determined observables were used in a

developed reconstruction algorithm which yields a sequence of contact points (of the vibrissa with the object) which describes a discrete reconstructed contour of the obstacle. The consideration of an elastic support of the vibrissa pointed out that the maximum bending moment can be restricted by an upper boundary (e.g. to avoid structural damage of the rod).

The investigations reported in this paper have to be continued towards more involved models. Animal vibrissae are not necessarily cylindrical as tacitly supposed here, but may be tapered and pre-curved in certain ways, and the objects are not necessarily strictly convex. Admitting such properties to the model makes the boundary value problems in general lose the nice feature to be autonomous. As a consequence, first integrals disappear and thereby a fully analytical representation of solutions is not possible anymore. An early numerical treatment of the boundary value problems is therefore inevitable. Nevertheless, to explore such improved models is necessary in order to understand the qualitative and quantitative effects which single or combined new ingredients of the models will generate. These are future tasks, partly already attacked.

A Representations by Standard Elliptic Integrals

In Section 5, the patient reader was staved off regarding the solution solution of multiple integrals. Now, we want to show how to get to an analytical expression of those. We define the elliptic integral of the first kind, analogous to [Abramowitz and Stegun, 1972, 17.2.7]:

$$\mathbb{F}(z,k) \coloneqq \int_0^z \frac{1}{\sqrt{1-t^2}\sqrt{1-k^2t^2}}\,\mathrm{d}t$$

and the elliptic integral of the second kind, analogous to [Abramowitz and Stegun, 1972, 17.2.8]:

$$\mathbb{E}(z,k) \coloneqq \int_0^z \sqrt{\frac{1-k^2t^2}{1-t^2}}\,\mathrm{d}t$$

Only in this subsection, the following abbreviations are used:

$$x = \varphi - \alpha, \quad u = \varphi_1 - \alpha, \quad \tau = t - \alpha\,.$$

In relation to the beams coordinate Y resp. X appears

$$J_s(\varphi,\varphi_0,\varphi_1,\alpha) \coloneqq \int_{\varphi_0}^{\varphi} \frac{\sin(t)}{\sqrt{\sin(t-\alpha)-\sin(\varphi_1-\alpha)}}\,\mathrm{d}t$$

$$J_c(\varphi,\varphi_0,\varphi_1,\alpha) \coloneqq \int_{\varphi_0}^{\varphi} \frac{\cos(t)}{\sqrt{\sin(t-\alpha)-\sin(\varphi_1-\alpha)}}\,\mathrm{d}t$$

with the previous defined abbreviations, J_s becomes

$$J_s = \cos(\alpha)\int_{\varphi_0-\alpha}^{x} \frac{\sin(\tau)}{\sqrt{\sin(\tau)-\sin(u)}}\,\mathrm{d}\tau + \sin(\alpha)\int_{\varphi_0-\alpha}^{x} \frac{\cos(\tau)}{\sqrt{\sin(\tau)-\sin(u)}}\,\mathrm{d}\tau\,.$$

We now define some auxiliary integrals:

$$I_s(x,\varphi_0,u) \coloneqq \int_{\varphi_0}^{x} \frac{\sin(\tau)}{\sqrt{\sin(\tau)-\sin(u)}}\,\mathrm{d}\tau\,, \qquad I_c(x,\varphi_0,u) \coloneqq \int_{\varphi_0}^{x} \frac{\cos(\tau)}{\sqrt{\sin(\tau)-\sin(u)}}\,\mathrm{d}\tau\,,$$

$$I_1(x,\varphi_0,u) \coloneqq \int_{\varphi_0}^{x} \frac{1}{\sqrt{\sin(\tau)-\sin(u)}}\,\mathrm{d}\tau\,, \qquad I_2(x,\varphi_0,u) \coloneqq \int_{\varphi_0}^{x} \sqrt{\sin(\tau)-\sin(u)}\,\mathrm{d}\tau\,.$$

By using some minor reshapes, we get

$$I_s(x,\varphi_0,u) = \sin(u) I_1(x,\varphi_0,u) + I_2(x,\varphi_0,u) \quad \text{and}$$
$$I_c(x,\varphi_0,u) = 2\left(\sqrt{\sin(x)-\sin(u)} - \sqrt{\sin(\varphi_0)-\sin(u)}\right).$$

Doing a straightforward calculation, we also get the formulas for I_1 and I_2.

$$\begin{aligned}
I_1 &= \int_{\varphi_0}^{x} \frac{1}{\sqrt{\cos\left(\tau-\frac{\pi}{2}\right)-\sin(u)}}\,\mathrm{d}\tau = \int_{\varphi_0-\frac{\pi}{2}}^{x-\frac{\pi}{2}} \frac{1}{\sqrt{\cos(\sigma)-\sin(u)}}\,\mathrm{d}\sigma \\
&= \int_{\varphi_0-\frac{\pi}{2}}^{x-\frac{\pi}{2}} \frac{1}{\sqrt{1-2\sin^2\left(\frac{\sigma}{2}\right)-\sin(u)}}\,\mathrm{d}\sigma, \quad \text{let} \quad k(u) \coloneqq \sqrt{\frac{1-\sin(u)}{2}}, \text{ then} \\
&= \frac{1}{\sqrt{2}k(u)} \int_{\varphi_0-\frac{\pi}{2}}^{x-\frac{\pi}{2}} \frac{1}{\sqrt{1-\frac{1}{k(u)^2}\sin^2\left(\frac{\sigma}{2}\right)}}\,\mathrm{d}\sigma, \quad \text{substitution:} \quad \sin\left(\frac{\sigma}{2}\right) = k(u)\,z \quad \text{yields} \\
&= \sqrt{2} \int_{\frac{1}{k(u)}\sin\left(\frac{\varphi_0}{2}-\frac{\pi}{4}\right)}^{\frac{1}{k(u)}\sin\left(\frac{x}{2}-\frac{\pi}{4}\right)} \frac{1}{\sqrt{(1-z^2)\left(1-k^2(u)z^2\right)}}\,\mathrm{d}z \\
&= \sqrt{2}\left(\int_{0}^{\frac{1}{k(u)}\sin\left(\frac{x}{2}-\frac{\pi}{4}\right)} \frac{1}{\sqrt{(1-z^2)\left(1-k^2(u)z^2\right)}}\,\mathrm{d}z - \int_{0}^{\frac{1}{k(u)}\sin\left(\frac{\varphi_0}{2}-\frac{\pi}{4}\right)} \frac{1}{\sqrt{(1-z^2)\left(1-k^2(u)z^2\right)}}\,\mathrm{d}z \right).
\end{aligned}$$

$$\begin{aligned}
I_2 &= \int_{\varphi_0-\frac{\pi}{2}}^{x-\frac{\pi}{2}} \sqrt{1-2\sin^2\left(\frac{\sigma}{2}\right)-\sin(u)}\,\mathrm{d}\sigma, \quad \text{let again } k(u) \coloneqq \sqrt{\frac{1-\sin(u)}{2}}, \text{ then} \\
&= \frac{2k(u)}{\sqrt{2}} \int_{\varphi_0-\frac{\pi}{2}}^{x-\frac{\pi}{2}} \sqrt{1-\frac{2}{k^2(u)}\sin^2\left(\frac{\sigma}{2}\right)}\,\mathrm{d}\sigma \quad \text{substitution:} \quad \sin\left(\frac{\sigma}{2}\right) = k(u)\,z \quad \text{yields} \\
&= \frac{4k^2(u)}{\sqrt{2}} \int_{\frac{1}{k(u)}\sin\left(\frac{\varphi_0}{2}-\frac{\pi}{4}\right)}^{\frac{1}{k(u)}\sin\left(\frac{x}{2}-\frac{\pi}{4}\right)} \frac{\sqrt{1-z^2}}{\sqrt{1-k^2(u)z^2}}\,\mathrm{d}z \\
&= 2\sqrt{2}\left(\int_{\frac{1}{k(u)}\sin\left(\frac{\varphi_0}{2}-\frac{\pi}{4}\right)}^{\frac{1}{k(u)}\sin\left(\frac{x}{2}-\frac{\pi}{4}\right)} \frac{1}{\sqrt{(1-z^2)\left(1-k^2(u)z^2\right)}}\,\mathrm{d}z \right. \\
&\qquad \left. - \left(1-k^2(u)\right) \int_{\frac{1}{k(u)}\sin\left(\frac{\varphi_0}{2}-\frac{\pi}{4}\right)}^{\frac{1}{k(u)}\sin\left(\frac{x}{2}-\frac{\pi}{4}\right)} \frac{\sqrt{1-k^2(u)z^2}}{\sqrt{1-z^2}}\,\mathrm{d}z \right)
\end{aligned}$$

So, I_1 and I_2 are

$$I_1(x,\varphi_0,u) = \sqrt{2}\left(\mathbb{F}\left(\frac{\sin\left(\frac{x}{2}-\frac{\pi}{4}\right)}{k(u)},k(u)\right)-\mathbb{F}\left(\frac{\sin\left(\frac{\varphi_0}{2}-\frac{\pi}{4}\right)}{k(u)},k(u)\right)\right)\ ,\ k(u)=\sqrt{\frac{1-\sin(u)}{2}}\,,$$

$$\begin{aligned} I_2(x,\varphi_0,u) = 2\sqrt{2}\Bigg(&\mathbb{E}\left(\frac{\sin\left(\frac{x}{2}-\frac{\pi}{4}\right)}{k(u)},k(u)\right)-\left(1-k(u)^2\right)\mathbb{F}\left(\frac{\sin\left(\frac{x}{2}-\frac{\pi}{4}\right)}{k(u)},k(u)\right)\\ &-\mathbb{E}\left(\frac{\sin\left(\frac{\varphi_0}{2}-\frac{\pi}{4}\right)}{k(u)},k(u)\right)+\left(1-k(u)^2\right)\mathbb{F}\left(\frac{\sin\left(\frac{\varphi_0}{2}-\frac{\pi}{4}\right)}{k(u)},k(u)\right)\Bigg)\,. \end{aligned}$$

Finally, we have as a comfortable way to handle the relevant objects of the theory the following:

$$\begin{aligned} K(\varphi,\varphi_0,\varphi_1,\alpha) &= -I_1(\varphi-\alpha,\varphi_0,\varphi_1-\alpha)+I_1\left(\varphi_0-\alpha,\varphi_0,\varphi_1-\alpha\right)\,,\\ X(\varphi;f,\varphi_0,\varphi_1,\alpha) &= \frac{1}{\sqrt{2f}}\Big(\sin(\alpha)\big(I_s(\varphi-\alpha,\varphi_0,\varphi_1-\alpha)-I_s\left(\varphi_0-\alpha,\varphi_0,\varphi_1-\alpha\right)\big)\\ &\qquad -\cos(\alpha)\big(I_c(\varphi-\alpha,\varphi_0,\varphi_1-\alpha)-I_c\left(\varphi_0-\alpha,\varphi_0,\varphi_1-\alpha\right)\big)\Big)\,,\\ Y(\varphi;f,\varphi_0,\varphi_1,\alpha) &= \frac{1}{\sqrt{2f}}\Big(-\cos(\alpha)\big(I_s(\varphi-\alpha,\varphi_0,\varphi_1-\alpha)-I_s\left(\varphi_0-\alpha,\varphi_0,\varphi_1-\alpha\right)\big)\\ &\qquad -\sin(\alpha)\big(I_c(\varphi-\alpha,\varphi_0,\varphi_1-\alpha)-I_c\left(\varphi_0-\alpha,\varphi_0,\varphi_1-\alpha\right)\big)\Big)\,. \end{aligned}$$

References

M. Abramowitz and I. A. Stegun. *Handbook of mathematical functions: With formulas, graphs, and mathematical tables*, volume 55 of *National Bureau of Standards applied mathematics series*. United States Department of Commerce, Washington and DC, 10. print., dec. 1972, with corr edition, 1972. ISBN 0471800074.

Daniel Baldeweg, Christoph Will, and Carsten Behn. Transversal Vibrations of Beams in Context of Vibrissae with Foundations, discrete Supports and various Sections. In Peter Scharff and Andrea Schneider, editors, *Shaping the future by engineering: 58th IWK, Ilmenau Scientific Colloquium, Technische Universität Ilmenau*, Ilmenau, Germany, 2014. Univ.-Verl. Ilmenau. ISBN 978-3-86360-085-3.

Carsten Behn. Modeling the Behavior of Hair Follicle Receptors as Technical Sensors using Adaptive Control. In Jean-Louis Ferrier, Jurek Sasiadek, Kurosh Madani, and Oleg Gusikhin, editors, *Proceedings of the 10th International Conference on Informatics in Control, Automation and Robotics*, pages 336–345. SCITEPRESS, 2013. ISBN 978-989-8565-70-9. doi: 10.5220/0004488003360345.

J. A. Birdwell, J. H. Solomon, M. Thajchayapong, M. A. Taylor, M. Cheely, R. B. Towal, J. Conradt, and M. J. Z. Hartmann. Biomechanical Models for Radial Distance Determination by the Rat Vibrissal System. *Journal of Neurophysiology*, 98(4):2439–2455, 2007. ISSN 0022-3077. doi: 10.1152/jn.00707.2006.

Yves Boubenec, Laure Nayelie Claverie, Daniel E. Shulz, and Georges Debrégeas. An amplitude modulation/demodulation scheme for whisker-based texture perception. *The Journal of neuroscience : the official journal of the Society for Neuroscience*, 34(33):10832–10843, 2014. ISSN 1529-2401. doi: 10.1523/JNEUROSCI.0534-14.2014.

T. N. Clements and C. D. Rahn. Three-dimensional contact imaging with an actuated whisker. *IEEE Transactions on Robotics*, 22(4):844–848, 2006. ISSN 1552-3098. doi: 10.1109/TRO.2006.878950.

S. Hirose, S. Inoue, and K. Yoneda. The whisker sensor and the transmission of multiple sensor signals. *Advanced Robotics*, 4(2):105–117, 1989. ISSN 0169-1864. doi: 10.1163/156855390X00099.

DaeEun Kim and Ralf Möller. Passive sensing and active sensing of a biomimetic whisker. In Luis M. Rocha, editor, *Artificial life X*, A Bradford book, pages 282–288. MIT Press, Cambridge, Mass, 2006. ISBN 978-0262681629.

DaeEun Kim and Ralf Möller. Biomimetic whiskers for shape recognition. *Robotics and Autonomous Systems*, 55(3):229–243, 2007. ISSN 09218890. doi: 10.1016/j.robot.2006.08.001.

Maria A. Neimark, M. L. Andermann, J. J. Hopfield, and C. I. Moore. Vibrissa Resonance as a Transduction Mechanism for Tactile Encoding. *J. Neurosci. (The Journal of neuroscience: the official journal of the Society for Neuroscience)*, 23(16):6499–6509, 2003. URL http://www.ncbi.nlm.nih.gov/pubmed/12878691.

Lorenz Pammer, Daniel H. O'Connor, S. Andrew Hires, Nathan G. Clack, Daniel Huber, Eugene W. Myers, and Karel Svoboda. The mechanical variables underlying object localization along the axis of the whisker. *The Journal of neuroscience : the official journal of the Society for Neuroscience*, 33(16):6726–6741, 2013. ISSN 1529-2401. doi: 10.1523/JNEUROSCI.4316-12.2013.

M. J. Pearson, B. Mitchinson, J. C. Sullivan, A. G. Pipe, and T. J. Prescott. Biomimetic vibrissal sensing for robots. *Philosophical Transactions of the Royal Society B: Biological Sciences*, 366 (1581):3085–3096, 2011. ISSN 0962-8436. doi: 10.1098/rstb.2011.0164.

Tony Prescott, Martin Pearson, Ben Mitchinson, J. Charles W. Sullivan, and Anthony Pipe. Whisking with robots: From Rat Vibrissae to Biomimetic Technology for Active Touch. *IEEE Robotics & Automation Magazine*, 16(3):42–50, 2009. ISSN 1070-9932. doi: 10.1109/MRA.2009.933624.

Brian W. Quist, Vlad Seghete, Lucie A. Huet, Todd D. Murphey, and Mitra J. Z. Hartmann. Modeling forces and moments at the base of a rat vibrissa during noncontact whisking and whisking against an object. *The Journal of neuroscience : the official journal of the Society for Neuroscience*, 34(30):9828–9844, 2014. ISSN 1529-2401. doi: 10.1523/JNEUROSCI.1707-12.2014.

Manuela Schmidt, Hartmut Witte, Klaus Zimmermann, Sandra Niederschuh, Thomas Helbig, Danja Voges, Isabel Husung, Tanja Volkova, Christoph Will, Carsten Behn, Joachim Steigenberger, and Gertrud Klauer. Technical, non-visual Characterization of Substrate Contact using Carpal Vibrissae as a Biological Model: an Overview. In Peter Scharff and Andrea Schneider, editors, *Shaping the future by engineering: 58th IWK, Ilmenau Scientific Colloquium, Technische Universität Ilmenau*, Ilmenau, Germany, 2014. Univ.-Verl. Ilmenau. ISBN 978-3-86360-085-3.

G. R. Scholz and C. D. Rahn. Profile Sensing With an Actuated Whisker. *IEEE Transactions on Robotics and Automation*, 20(1):124–127, 2004. ISSN 1042-296X. doi: 10.1109/TRA.2003.820864.

Joachim Steigenberger, Carsten Behn, and Christoph Will. Mathematical model of vibrissae for surface texture detection. Preprint No. M15/03, Faculty of Mathematics and Natural Sciences, TU Ilmenau, 2015. URL http://www.db-thueringen.de/servlets/DocumentServlet?id=25964.

C. Tuna, J. H. Solomon, D. L. Jones, and M. J. Z. Hartmann. Object shape recognition with artificial whiskers using tomographic reconstruction. In *IEEE International Conference on*

Acoustics, Speech and Signal Processing (ICASSP), pages 2537–2540, Piscataway, NJ, 2012. IEEE. ISBN 978-1-4673-0046-9. doi: 10.1109/ICASSP.2012.6288433.

Danja Voges, Kathrin Carl, Gertrud J. Klauer, René Uhlig, Cornelius Schilling, Carsten Behn, and Hartmut Witte. Structural Characterization of the Whisker System of the Rat. *IEEE Sensors Journal*, 12(2):332–339, 2012. ISSN 1530-437X. doi: 10.1109/JSEN.2011.2161464.

Christoph Will, Joachim Steigenberger, and Carsten Behn. Object Contour Reconstruction using Bio-inspired Sensors. In Joaquim Filipe, Jurek Sasiadek, Kurosh Madani, and Oleg Gusikhin, editors, *Proceedings of the 11th International Conference on Informatics in Control, Automation and Robotics*, pages 459–467. SCITEPRESS, 2014a. ISBN 978-989-758-039-0. doi: 10.5220/0005018004590467.

Christoph Will, Joachim Steigenberger, and Carsten Behn. Quasi-static object scanning using technical vibrissae. In Peter Scharff and Andrea Schneider, editors, *Shaping the future by engineering: 58th IWK, Ilmenau Scientific Colloquium, Technische Universität Ilmenau*, Ilmenau, Germany, 2014b. Univ.-Verl. Ilmenau. ISBN 978-3-86360-085-3.